THE JOURNAL OF BIOLOGICAL CHEMISTRY VOL. 287, NO. 25, pp. 21233–21243, June 15, 2012

β-Subunit of the Ostα-Ostβ Organic Solute Transporter Is Required Not Only for Heterodimerization and Trafficking but Also for Function*[S]

Received for publication, February 11, 2012, and in revised form, April 9, 2012 Published, JBC Papers in Press, April 25, 2012, DOI 10.1074/jbc.M112.352245

Whitney V. Christian[‡], Na Li[‡], Patricia M. Hinkle[§1], and Nazzareno Ballatori[†‡]

From the Departments of [‡]Environmental Medicine and [§]Pharmacology and Physiology, University of Rochester School of Medicine, Rochester, New York 14642

Background: Deletion of Ostα-Ostβ, an intestinal transporter that participates in the enterohepatic circulation of bile acids, lowers cholesterol and triglyceride levels.
Results: Residues of Ostβ required for interaction with Ostα and transport activity were identified.
Conclusion: Distinct regions of Ostβ are essential for Ostα-Ostβ trafficking and transport activity.
Significance: Findings suggest strategies for inhibiting the holotransporter and reducing lipid levels.

The organic solute transporter, Ost/Slc51, is composed of two distinct proteins that must heterodimerize to generate transport activity, but the role of the individual subunits in mediating transport activity is unknown. The present study identified regions in Ostβ required for heterodimerization with Ostα, trafficking of the Ostα-Ostβ complex to the plasma membrane, and bile acid transport activity in HEK293 cells. Bimolecular fluorescence complementation analysis revealed that a 25-amino acid peptide containing the Ostβ transmembrane (TM) domain heterodimerized with Ostα, although the resulting complex failed to reach the plasma membrane and generate cellular [^{3}H]taurocholate transport activity. Deletion of the single TM domain of Ostβ abolished interaction with Ostα, demonstrating that the TM segment is necessary and sufficient for formation of a heteromeric complex with Ostα. Mutation of the highly conserved tryptophan-asparagine sequence within the TM domain of Ostβ to alanines did not prevent cell surface trafficking, but abolished transport activity. Removal of the N-terminal 27 amino acids of Ostβ resulted in a transporter complex that reached the plasma membrane and exhibited transport activity at 30 °C. Complete deletion of the C terminus of Ostβ abolished [^{3}H]taurocholate transport activity, but reinsertion of two native arginines immediately C-terminal to the TM domain rescued this defect. These positively charged residues establish the correct N_{exo}/C_{cyt} topology of the peptide, in accordance with the positive inside rule. Together, the results demonstrate that Ostβ is required for both proper trafficking of Ostα and formation of the functional transport unit, and identify specific residues of Ostβ critical for these processes.

The heteromeric organic solute transporter (Ost)[2] α-β (Ostα-Ostβ/Slc51) is the key basolateral plasma membrane bile acid and steroid conjugate carrier in many human tissues, including the small intestine, liver, and other steroidogenic organs (1–4). Recently, *Ostα*$^{-/-}$ mice have been generated (5–7), and these animals exhibit a major defect in intestinal bile acid absorption, confirming that Ostα-Ostβ is the main intestinal bile acid efflux transporter in the enterohepatic circulation. Bile acids, which are major products of cholesterol catabolism, are required for hepatic bile secretion and for the emulsification and intestinal absorption of fat and fat-soluble vitamins (8). To better understand the biological roles of the two subunits and to gather biomolecular information potentially useful in developing strategies for modulating transport activity, studies were undertaken to investigate the role of mouse Ostβ in the holotransporter.

The overall structure of Ostα-Ostβ resembles that of certain G protein-coupled receptors, including the G protein-coupled receptor-receptor activity-modifying protein (GPCR-RAMP) complexes. Ostβ, a 128-amino acid protein in humans and mice, is predicted to contain a single transmembrane (TM) domain, and to be oriented in the plasma membrane with its N terminus in the extracellular space and its C terminus in the cytosol (N_{exo}/C_{cyt} with no signal peptide, classified as a type Ia integral membrane protein) (5). Although its complete biological function(s) in the heteromeric complex has not yet been established, Ostβ appears to serve as a chaperone facilitating the cell surface delivery of the 7-TM domain Ostα subunit,

* This work was supported, in whole or in part, by National Institute of Health Grants DK067214, DK48823, and DK19974 and NIEHS/National Institutes of Health Training Grant ES07026 and Center Grants ES03828 and ES01247. This work has been partially published in abstract form (Christian, W. V., Li, N., and Ballatori, N. (2011) *FASEB J.* **25**, 554.1).
[S] This article contains supplemental Table S1 and Figs. S1–S4.
This work is dedicated to our beloved colleague Nazzareno Ballatori, Ph.D., who discovered Ostα-Ostβ. Dr. Ballatori died during the preparation of this manuscript; he is deeply missed.
[†] Deceased, December 25, 2011.
[1] To whom correspondence should be addressed: Dept. of Pharmacology and Physiology, Box 711, University of Rochester School of Medicine, 601 Elmwood Ave., Rochester, NY 14642. Tel.: 585-275-4933; Fax: 585-273-2652; E-mail: patricia_hinkle@urmc.rochester.edu.

[2] The abbreviations used are: Ost, organic solute transporter; BiFC, bimolecular fluorescence complementation; C_{cyt}, cytosolic C terminus; ER, endoplasmic reticulum; HBSS, Hanks' balanced salt solution; N_{exo}, extracellular N terminus; *N***N**, glycosylation tag; PNGase F, peptide:*N*-glycosidase F; TM, transmembrane; Tricine, *N*-[2-hydroxy-1,1-bis(hydroxymethyl)-ethyl]glycine; V5, epitope tag from the P and V proteins of simian virus 5; YC, YFP residues 156–238; YN, YFP residues 1–155.

presumed to be the main catalytic subunit of the transporter (5, 9, 10).

Co-expression of Ostα and Ostβ is required to elicit transport activity (4, 11, 12), and Li *et al.* (5) have demonstrated that Ostα and Ostβ are present in cells as heterodimers and/or heteromultimers. Heterodimerization of Ostα and Ostβ increases the stability of the individual proteins and is required for delivery of the heteromeric complex to the plasma membrane (5). Formation of the transporter complex is also coupled to post-translational modifications of Ostα; *i.e.* stable interaction between the subunits is required for progression through the biosynthetic-secretory pathway and to generate a glycosylated form of Ostα (5, 9, 10). Thus, the glycosylation status of Ostα can be utilized as an index of interaction between the two subunits.

Interestingly, although skate Ostβ and human OSTβ display roughly 25% amino acid identity, previous studies have shown that human OSTα can generate comparable taurocholate transport activity when complemented with either human OSTβ or skate Ostβ, suggesting that only a few conserved amino acids or the secondary structure of the OSTβ/Ostβ proteins is important for interaction (4). The goal of this work was to identify regions of Ostβ that are critical for dimerization with Ostα, trafficking, and transport activity. The three main amino acid segments of Ostβ were analyzed: (i) C-terminal residues 54–107; (ii) N-terminal residues 1–27; and (iii) the TM domain region. In addition, point mutants of evolutionarily conserved residues in Ostβ were constructed and characterized.

EXPERIMENTAL PROCEDURES

Materials—HEK293 cells (ATCC, CRL-1573) were grown as monolayers at 37 °C, unless otherwise indicated, in an atmosphere of 5% CO_2. Cells were maintained in DMEM (GIBCO) containing 10% FBS and antibiotics. [^{3}H]Taurocholic acid (2 Ci/mmol) was purchased from PerkinElmer Life Sciences.

Production of Mutant Ostβ Proteins—Ostα, Ostβ, and the truncations of Ostβ were amplified via PCR using primers shown in supplemental Table S1 and inserted into pcDNA3.3 (Invitrogen). Ostβ-Δ34–53, the Ostβ point mutants, Ostβ-1–55, and Ostβ-1–55 R54A/R55A were generated by site-directed mutagenesis using QuikChange (Stratagene). All constructs were sequenced for accuracy.

Transient Expression in HEK293 Cells and Bile Acid Transport Activity Assay—HEK293 cells in 6-well plates were transfected with 900 ng of Ostα and 100 ng of each Ostβ species DNA using LipoD293 (SignaGen). Twelve h later, the medium was replaced, and cells were incubated at 30 °C or 37 °C for an additional 36 h. At 48 h after transfection, medium was replaced with Hanks' balanced salt solution (HBSS) (Invitrogen) containing 25 μM [^{3}H]taurocholic acid, and cells were incubated at 37 °C for 30 min. After incubation, cells were washed twice with ice-cold HBSS containing 1 mM unlabeled taurocholate and 0.2% (w/v) BSA and then once with ice-cold HBSS alone. Monolayers were lysed overnight in 1 N NaOH, and an aliquot of the transport media and the lysate was analyzed by liquid scintillation to assess transport activity. Lysate protein concentrations were determined with the DC protein assay (Bio-Rad), and nonspecific cell-associated radioactivity was accounted for by subtracting radioactivity detected at time zero.

Construction and Visualization of Fluorescent Fusion Proteins—For bimolecular fluorescence complementation (BiFC) analysis (13–15), residues 1–155 of YFP (YN) were fused to the C terminus of Ostα, and residues 156–238 of YFP (YC) were fused to the C terminus of each Ostβ construct. Ostα-YN in pBiFCN and Ostβ-YC in pBiFCC were described previously (5). Truncations of Ostβ were PCR-amplified and ligated into pBiFCC. Constructs in pBiFCN/pBiFCC were then subcloned into pcDNA3.3. BiFC-tagged Ostβ point mutants were produced via site-directed mutagenesis. Cerulean (from Dr. David Piston, Vanderbilt University) was PCR-amplified and ligated 3′ to Ostα. The two halves of YFP in pBiFCN and pBiFCC were combined 3′ to Ostβ, generating Ostβ-YFP. Two rounds of mutagenesis were conducted to change the YFP coding sequence to Topaz (16). The Topaz coding sequence was then PCR-amplified and ligated 3′ to Ostβ mutants. Stop codons in the linkers were changed to alanine codons via site-directed mutagenesis.

For visualization, HEK293 cells on glass-bottom Petri dishes (Mat-Tek) were transfected with 900 ng of Ostα-YN/Cerulean and 100 ng of each Ostβ species-YC/Topaz DNA. Twelve h later, the medium was replaced, and cells were incubated at 30 °C (BiFC) or 37 °C (Cerulean/Topaz) for 36 h. At 48 h after transfection, cells were incubated at 37 °C for 15 min in HBSS containing 2 μg/ml wheat germ agglutinin-Alexa Fluor 647 conjugate, 2 μM Hoechst 33342, and 2 μM ER-Tracker Red (all from Molecular Probes). Cells were then washed and visualized in imaging buffer (136 mM NaCl, 560 μM $MgCl_2$, 4.7 mM KCl, 1 mM Na_2HPO_4, 10 mM HEPES, 5.5 mM glucose, and 1.3 mM $CaCl_2$, pH 7.4) with an FV1000 Olympus laser scanning confocal microscope using a 60×objective. Imaging was conducted with virtual channels in two phases: (i) Hoechst 33342 (405 nm excitation, 425/456 nm emission), ER-Tracker Red (559 nm, 575/620 nm), and wheat germ agglutinin 647 (635 nm, 655/755 nm); and (ii) Cerulean (440 nm, 472/497 nm) and YFP/Topaz (515 nm, 530/585 nm). Sequential scanning was used for both phases, and saturation was controlled through the FV1000 software.

N-terminal Epitope Tagging of Constructs and Cell Surface ELISA—The N termini of Ostα and Ostβ were tagged with V5 and triple HA (3×HA) epitopes, respectively, via site-directed mutagenesis. HEK293 cells were transfected with 900 ng of V5-Ostα and 100 ng of each 3×HA-Ostβ species DNA in 24-well plates. At 48 h after transfection, cell surface ELISA was conducted as described previously (17). Briefly, plates were incubated with monoclonal anti-V5 (Invitrogen) and anti-HA (Covance) at 1:5,000 followed by anti-mouse IgG-HRP (Bio-Rad) at 1:5,000. Antibody binding was detected with 3,3′5,5′-tetramethylbenzidine, and the reaction was terminated with 10% sulfuric acid. Absorbance was read at 450 nm, and values from duplicate points were averaged. Absorbance in mock-transfected cells was subtracted, and the resulting values were normalized to those obtained in V5-Ostα-3×HA-Ostβ-transfected cells, which were present on each plate.

Whole Cell Lysate Preparation and Immunoblotting—At 48 h after transfection, HEK293 cells were lysed with PBS containing

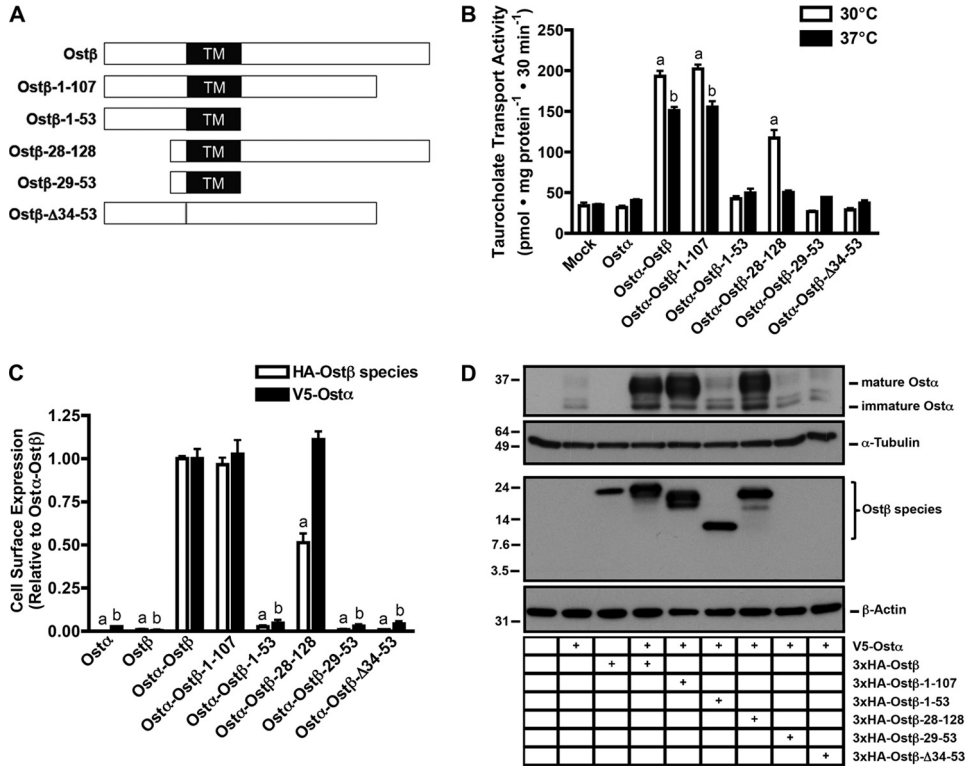

FIGURE 1. **Importance of different domains of Ostβ.** *A*, Ostβ truncations. The *black bar* symbolizes the predicted single TM domain. *B*, [^{3}H]taurocholate transport activity generated by the indicated pairings of untagged constructs. *a* and *b*, $p < 0.05$ *versus* mock-transfected cells at 30 or 37 °C, respectively. *Error bars*, S.E. *C*, relative cell surface expression of V5-Ostα and the 3×HA-Ostβ truncations determined by ELISA. *a*, $p < 0.05$ *versus* 3×HA-Ostβ when co-expressed with V5-Ostα; *b*, $p < 0.05$ *versus* V5-Ostα when co-expressed with 3×HA-Ostβ. *D*, immunoblots of V5-Ostα and 3×HA-Ostβ mutants. V5-Ostα was visualized with mouse monoclonal anti-V5 antibody followed by HRP-labeled secondary antibody and 3×HA-Ostβ truncations with rat anti-HA-HRP.

1% (v/v) protease inhibitor mixture (Sigma), 5 mM EDTA, 2 mM PMSF, and 0.2% Triton X-100. Lysates were centrifuged at 20,000 × *g* for 15 min at 4 °C, and the supernatant was taken as the whole cell lysate and immediately frozen at −80 °C. Lysate protein concentrations were determined with the DC protein assay.

For immunoblotting of V5-Ostα, 15 μg of each sample was subjected to Laemmli-SDS-PAGE on 10% Tris-HCl ready gels (Bio-Rad) followed by wet transfer onto PVDF using Dunn carbonate buffer (10 mM $NaHCO_3$, 3 mM Na_2CO_3, pH 9.9, 20% methanol) for 90 min at 100 volts. Blots were blocked in milk at room temperature for 3 h and then incubated at 4 °C overnight with anti-V5 at 1:10,000. Anti-mouse IgG-HRP (KPL) at 1:5,000 was then applied for 1 h at room temperature. For immunoblotting of 3×HA-Ostβ mutants, 15 μg of each sample was subjected to Tricine-SDS-PAGE on 10–20% or 16.5% Tris-Tricine precast gels (Bio-Rad) followed by wet transfer using Towbin buffer (Bio-Rad). Blots were blocked overnight at 4 °C and then incubated with anti-HA HRP conjugate (Roche Applied Science) at 25 milliunits/ml for 1 h at room temperature. Antibody binding was detected with LumiGLO Peroxidase Chemiluminescent Substrate (KPL). For loading controls, blots were probed with anti-α-tubulin or anti-β-actin (Sigma).

N_{exo}/C_{cyt} Topology Assessment—Glycosylation tags (*N*N**) were added to the N termini of constructs via mutagenic PCR. The glycosylation tag is a segment of the *Saccharomyces cerevisiae* α-factor receptor Ste2p with the amino acid sequence STI-**N**YTSIYG**N**GSTITSSS, which contains two Asn residues that are known to be *N*-glycosylated when luminal in the ER (18). HEK293 cells were transiently transfected with 900 ng of V5-Ostα and 100 ng of each *N*N**-3×HA-Ostβ species DNA, and whole cell lysates were collected 48 h later. Protein samples were processed with the Glycoprofile II, Enzymatic In-Solution *N*-Deglycosylation kit (Sigma) and subjected to SDS-PAGE for band shift analysis.

Statistical Analyses—All bar graphs show the mean ± S.E. from three or four independent experiments, each performed in duplicate or triplicate. Data were evaluated with Prism 4 using one-way ANOVA followed by Bonferroni's multiple comparison test, or the two-tailed unpaired Student's *t* test. Differences were considered statistically significant at $p < 0.05$. Sequences were aligned using the MUSCLE program (multiple sequence comparison by log-expectation).

RESULTS

Domains of Ostβ Required for Function—To identify regions of Ostβ that are important for function, five truncation mutants were constructed (Fig. 1*A*). These Ostβ truncations were transiently transfected into HEK293 cells with Ostα, and [^{3}H]taurocholate transport activity was measured (Fig. 1*B*). To correlate functional and visualization results with the BiFC-tagged proteins, cells were incubated at either 30 or 37 °C before transport activity was measured (see below).

As expected, cells co-expressing wild-type Ostα and Ostβ demonstrated robust taurocholate uptake (Fig. 1*B*). Deletion of the 21 C-terminal residues of Ostβ, generating Ostβ-1–107,

did not affect transport activity; however, complete truncation of the C terminus, yielding Ostβ-1–53, markedly decreased taurocholate uptake (Fig. 1*B*). Deletion of the N terminus of Ostβ, producing Ostβ-28–128, resulted in a heteromeric transporter complex that elicited transport activity, but only if cells were incubated at 30 °C. Transport activity of the wild-type heteromer was also slightly higher if cells were incubated at 30 °C (Fig. 1*B*). Culturing at low temperatures is known to increase protein production (19–23) and rescue function of some mutant transporters (24, 25). No transport activity was detected when Ostα was expressed with mutants of Ostβ that contained only the TM domain region (Ostβ-29–53) or lacked the entire TM domain (Ostβ-Δ34–53) (Fig. 1*B*).

To determine whether the loss of transport activity observed with these Ostβ mutants was due to failure of the resulting transporter complex to traffic to the plasma membrane, Ostα and the truncated Ostβs were tagged at the N termini with V5 and triple HA (3×HA) epitopes, respectively, and the amounts of these proteins at the cell surface were determined (Fig. 1*C*). The tagged proteins gave taurocholate transport activity comparable with, although somewhat lower than, their untagged counterparts (compare Fig. 1*B* and supplemental Fig. S1), as observed previously (5). As expected, neither 3×HA-Ostβ nor V5-Ostα was found at the cell surface when expressed alone. When expressed with V5-Ostα, the Ostβ constructs that displayed transport activity (3×HA-Ostβ, 3×HA-Ostβ-1–107, and 3×HA-Ostβ-28–128) were readily detected at the plasma membrane along with the V5-Ostα subunit, although 3×HA-Ostβ-28–128 was present at half the level of the full-length protein even though V5-Ostα was detected in normal amounts (Fig. 1*C*). One possible explanation for this result is that the 3×HA tag on 3×HA-Ostβ-28–128 is closer to the TM domain of Ostβ and may be partially occluded in the resulting V5-Ostα-3×HA-Ostβ-28–128 heteromer. The Ostβ constructs that did not give transport activity (3×HA-Ostβ-1–53, 3×HA-Ostβ-29–53, and 3×HA-Ostβ-Δ34–53) were not localized at the plasma membrane, nor was co-expressed V5-Ostα (Fig. 1*C*), explaining the absence of functional activity.

The Ostβ constructs that were detected at the plasma membrane (3×HA-Ostβ, 3×HA-Ostβ-1–107, and 3×HA-Ostβ-28–128) gave strong bands on immunoblots when expressed with V5-Ostα (Fig. 1*D*). V5-Ostα was also present at high levels and appeared fully glycosylated, indicating that it had been post-translationally modified in the Golgi apparatus upon interaction with the Ostβ constructs. In contrast, 3×HA-Ostβ-1–53, which was not detectable on the cell surface, was visible on immunoblots; however, in this pairing V5-Ostα was largely absent and not fully glycosylated (Fig. 1*D*). Neither 3×HA-Ostβ-29–53 nor 3×HA-Ostβ-Δ34–53 was detected on immunoblots (Fig. 1*D*), suggesting that these mutants are unstable.

BiFC Analysis of Ostα-Ostβ Interaction—To observe the interaction between Ostα and Ostβ and its subcellular localization simultaneously in live cells, BiFC analysis was conducted using confocal microscopy. The N-terminal half of YFP (YN) was fused to the C terminus of Ostα and the C-terminal half of YFP (YC) to the C terminus of each Ostβ species. If Ostα and Ostβ interact directly, the two halves of the fluorophore form YFP. The BiFC constructs exhibited taurocholate transport activity roughly comparable with that of the untagged constructs (compare Figs. 1*B* and 2*A*). One interesting exception was Ostβ-1–53-YC, which showed significant transport activity upon co-expression with Ostα-YN (Fig. 2*A*), whereas their untagged counterparts did not (Fig. 1*B*).

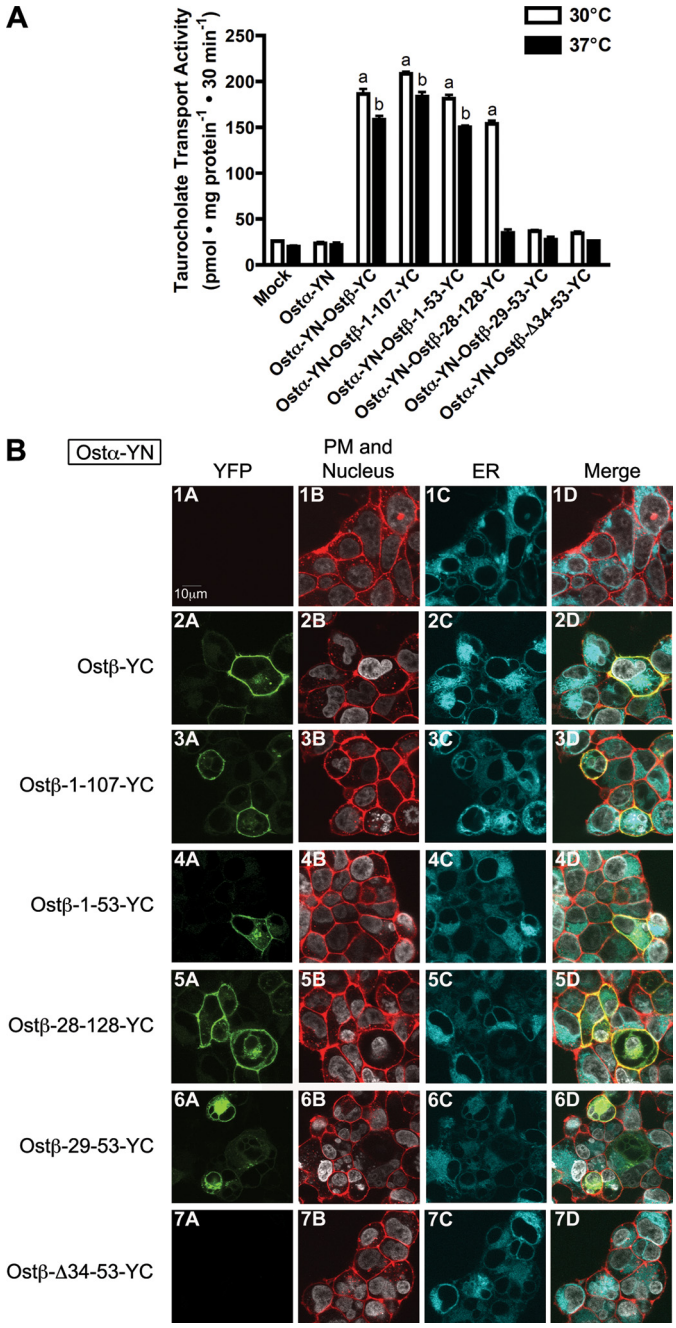

FIGURE 2. **Analysis of Ostα-Ostβ interactions in live cells.** *A*, uptake of 25 μM [^{3}H]taurocholate by proteins tagged for BiFC analysis. *a* and *b*, $p < 0.05$ *versus* mock-transfected cells at 30 or 37 °C, respectively. *Error bars*, S.E. *B*, BiFC analysis in live cells. Ostα-YN was co-expressed with the indicated YC-tagged Ostβ constructs. *A*, YFP (BiFC), *green*; *B*, plasma membrane (*PM*) and nucleus, *red* and *gray*, respectively; *C*, ER, *blue*; and *D*, merge all. *Scale bar*, 10 μm.

Ostβ-YC, Ostβ-1–107-YC, and Ostβ-28–128-YC showed clear YFP fluorescence at the plasma membrane, indicating that they heterodimerized with Ostα-YN and trafficked to the cell surface (Fig. 2*B*). These findings are consistent with surface expression measurements described above. In contrast with the

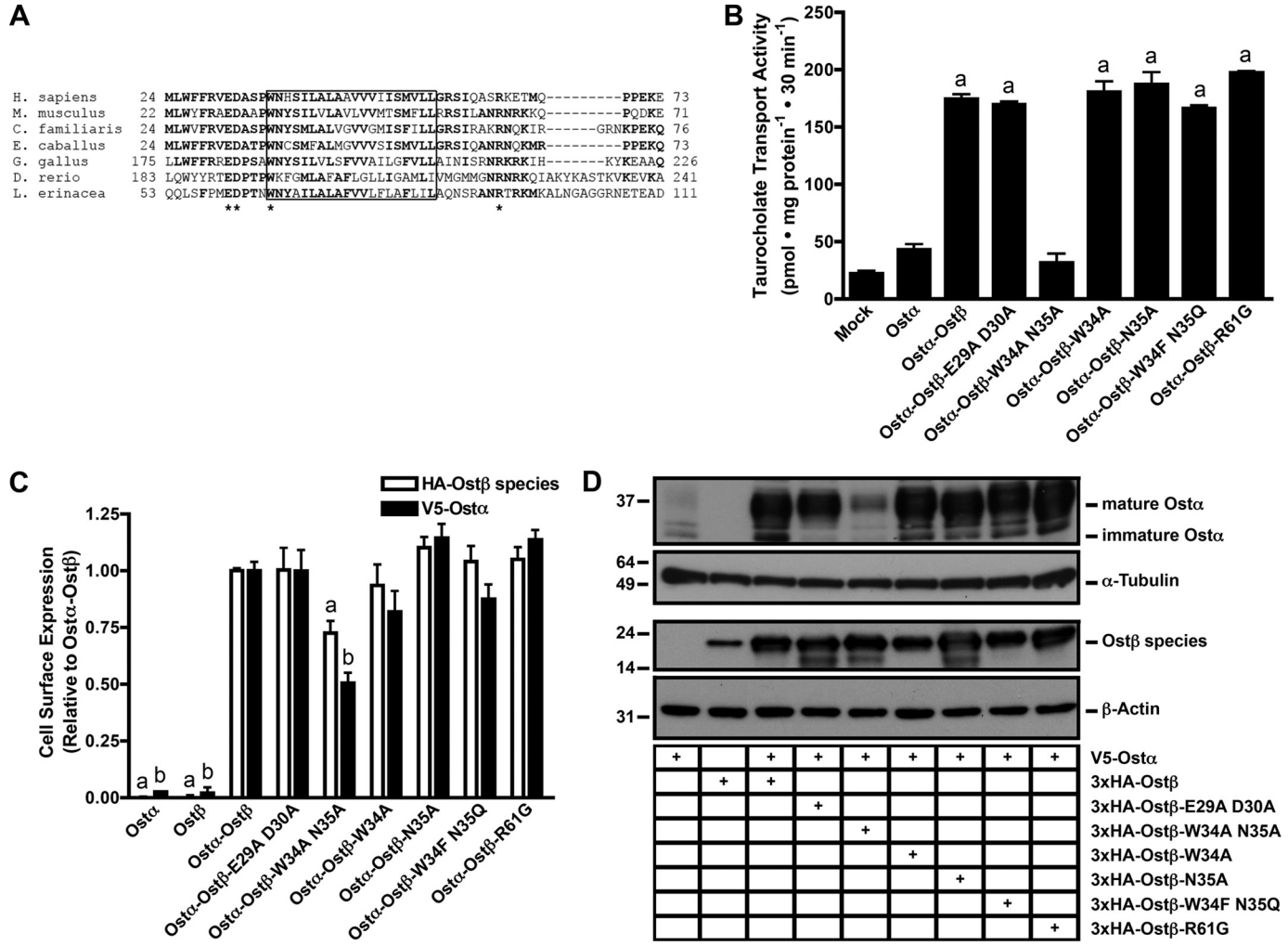

FIGURE 3. **Function of conserved residues of Ostβ.** *A*, alignment of human, mouse, dog, horse, chicken, zebrafish, and skate Ostβ proteins. Amino acid identity is *boldface*, and the predicted TM domain is *boxed*. *Asterisks* denote conserved amino acids. *B*, [^{3}H]taurocholate transport activity generated by Ostα paired with each Ostβ point mutant. *a*, $p < 0.05$ *versus* mock-transfected cells. *Error bars*, S.E. *C*, relative cell surface localization of each protein as determined via ELISA. *a*, $p < 0.05$ *versus* 3×HA-Ostβ when co-expressed with V5-Ostα; *b*, $p < 0.05$ *versus* V5-Ostα when co-expressed with 3×HA-Ostβ. *D*, immunoblots of V5-Ostα and 3×HA-Ostβ point mutants.

behavior of the epitope-tagged proteins, Ostβ-1–53-YC and Ostα-YN heterodimerized at the plasma membrane (Fig. 2*B*), consistent with the transport activity generated by this complex (Fig. 2*A*). Ostβ-29–53-YC (TM domain region of Ostβ only) and Ostα-YN formed a BiFC complex that was retained in the ER (Fig. 2*B*), in accord with the lack of detectable complex on the cell surface (Fig. 1*C*). The Ostβ complex lacking the TM region (Ostβ-Δ34–53-YC) did not interact with Ostα-YN (Fig. 2*B*), in agreement with surface expression and immunoblotting data (Fig. 1, *B* and *D*). These findings suggest that the TM domain of Ostβ is sufficient for interaction with Ostα but not for trafficking.

To ensure that these findings did not result from the affinity of the YFP fragments for one another, the fluorophores Cerulean and Topaz, which exhibit no affinity for each other, were fused to the C termini of Ostα and the Ostβ truncations, respectively. The Topaz fusions of Ostβ, Ostβ-1–107, Ostβ-1–53, and Ostβ-28–128 all co-localized with Ostα-Cerulean at the plasma membrane (supplemental Fig. S2), in agreement with the BiFC results (Fig. 2*B*). Ostβ-29–53-Topaz (TM domain region only) and Ostβ-Δ34–53-Topaz (no TM domain) were detected in cells (supplemental Fig. S2), whereas the 3×HA-tagged versions were not (Fig. 1*D*). This is not surprising because GFP and its variants tend to increase the stability of proteins (26–29). Ostα-Cerulean and Ostβ-29–53-Topaz co-localized in the ER (supplemental Fig. S2), in agreement with BiFC results. Ostβ-Δ34–53-Topaz, which lacks a TM region, exhibited a diffuse intracellular localization, whereas Ostα-Cerulean remained in the ER (supplemental Fig. S2).

Ostβ Participates in Transport Mechanism—Additional studies examined the evolutionarily conserved amino acids in Ostβ to determine their role in transport activity. Sequence alignment of Ostβs from seven different species (1) revealed that the TM domain and several amino acids in close proximity to this membrane helix are most conserved (Fig. 3*A*). Four residues are completely conserved: a Glu-Asp sequence (Glu^{29}-Asp^{30}) near the N terminus of the TM helix, a Trp (Trp^{34}) at the predicted start of the TM domain, and an Arg (Arg^{61}) located eight amino acids from the C terminus of the TM domain. Also of note is the highly conserved Asn

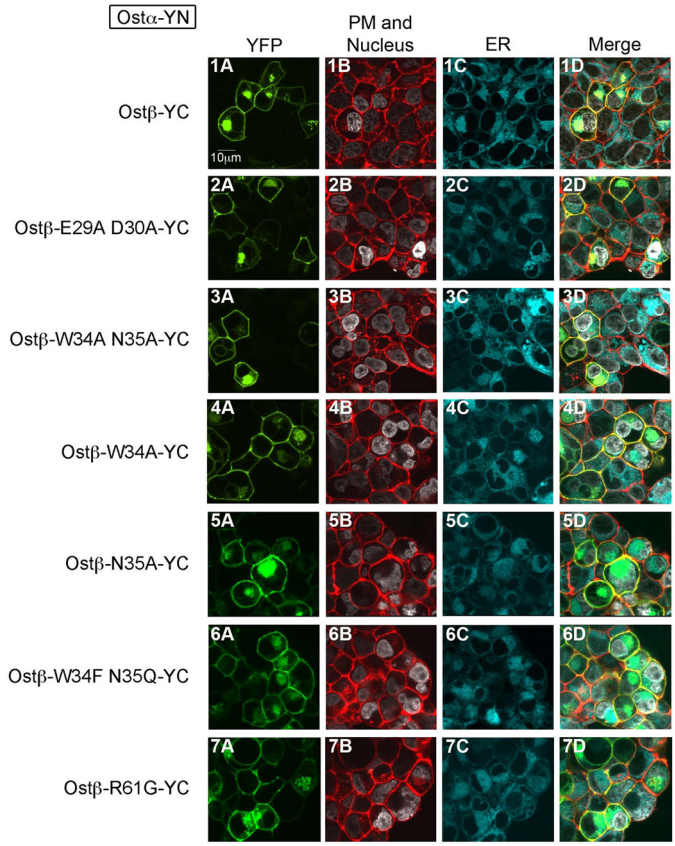

FIGURE 4. **Ostβ point mutants interact with Ostα and localize at the plasma membrane (*PM*).** BiFC analysis of Ostα-YN expressed with the indicated YC-tagged Ostβ point mutants is shown. *A*, YFP (BiFC), *green*; *B*, plasma membrane and nucleus, *red* and *gray*, respectively; *C*, ER, *blue*; and *D*, merge all. *Scale bar*, 10 μm.

(Asn^{35}), which is present in all species except the zebrafish (Fig. 3*A*). Site-directed mutagenesis was conducted to produce Ostβ-E29A D30A, Ostβ-W34A/N35A, Ostβ-W34A, Ostβ-N35A, and Ostβ-R61G, and each construct was expressed with Ostα. All constructs exhibited transport activity except for the Ostβ mutant in which the highly conserved Trp-Asn sequence at the beginning of the TM segment was mutated to Ala-Ala (Fig. 3*B*). When this Trp-Asn sequence was mutated to Phe-Gln (Ostβ-W34F/N35Q), function was intact (Fig. 3*B*). Despite their inability to form a functional transporter, V5-Ostα and 3×HA-Ostβ-W34A/N35A were detected at the plasma membrane at ~50 and 75% of wild-type levels, respectively (Fig. 3*C*). Immunoblotting showed that the expression of the Ostβ point mutants was equivalent although the presence of fully glycosylated V5-Ostα was decreased when it was paired with 3×HA-Ostβ-W34A/N35A, suggesting that this mutant may have difficulty interacting with Ostα (Fig. 3*D*).

To examine interactions of these Ostβ mutants with Ostα directly, BiFC-tagged versions were analyzed by fluorescence microscopy (Fig. 4), as were Cerulean- and Topaz-tagged constructs (supplemental Fig. S3). Both BiFC and co-localization approaches showed that all of the Ostβ point mutants localized at the plasma membrane and interacted with Ostα, including the functionally inactive Ostβ-W34A/N35A.

Importance of C Terminus of Ostβ for Cell Surface Localization—As shown above, untagged Ostβ-1–53, which lacks the entire region C-terminal to the TM domain, failed to traffic to the cell surface or generate transport activity (Fig. 1 and supplemental Fig. S1). Conversely, Ostβ-1–53 tagged at the C terminus with YC or Topaz did traffic to the plasma membrane (Fig. 2*B* and supplemental Fig. S3) and exhibit taurocholate transport activity (Fig. 2*A* and data not shown), suggesting that the fused fluorophores can replace the natural amino acids 54–107. To characterize the function(s) of the C terminus more precisely, successive truncations were made, generating Ostβ-1–103, 1–93, 1–83, 1–73, and 1–63 (Fig. 5*A*). When these constructs were co-expressed with Ostα, all generated transport activity (Fig. 5*B*). Although Ostα-Ostβ-1–53 was inactive, addition of the two natural Arg residues at positions 54 and 55 restored transport activity; however, substitution with two Ala residues, giving Ostβ-1–55 R54A/R55A, resulted in a loss of transport activity (Fig. 5*B*).

Cell surface ELISA was utilized to detect the presence of 3×HA-tagged versions of these constructs at the plasma membrane. Interestingly, as the C terminus of Ostβ was progressively shortened, surface levels of both the mutant 3×HA-Ostβ and V5-Ostα declined (Fig. 5*C*). Although almost no 3×HA-Ostβ-1–53 was detected at the plasma membrane, adding back the two Arg residues (3×HA-Ostβ-1–55) restored surface expression and transport activity, whereas adding two Ala residues did not (Fig. 5*C*). In cells expressing Ostβ-1–55, [^{3}H]taurocholate uptake was equivalent to that obtained with wild-type Ostβ (Fig. 5*B*), even though surface expression of both V5-Ostα and 3×HA-Ostβ-1–55 was lower. This result is consistent with the correlation between the levels of wild-type V5-Ostα and 3×HA-Ostβ on the plasma membrane and transport activity. Transport activity reached a maximum before surface expression of V5-Ostα or 3×HA-Ostβ when cells were transfected with a constant amount of cDNA encoding V5-Ostα and increasing amounts of cDNA encoding 3×HA-Ostβ (supplemental Fig. S4).

Immunoblotting revealed that the 3×HA-Ostβ C-terminal mutant proteins were present at roughly comparable levels; however, the expression of V5-Ostα and its fully glycosylated form decreased as the C terminus was shortened or replaced with two Ala residues (3×HA-Ostβ-1–55 R54A/R55A) (Fig. 5*D*). These results indicate that the two residues just C-terminal to the TM region of Ostβ-1–55, Arg^{54} and Arg^{55}, were sufficient for proper membrane localization and activity.

Positively Charged Residues in C Terminus of Ostβ Establish Its N_{exo}/C_{cyt} Topology—Positively charged residues flanking the TM domain of integral membrane proteins are major determinants of topology (30–33), with the positively charged side typically oriented toward the cytoplasm (positive inside rule). To examine whether Arg^{54} and Arg^{55} establish a N_{exo}/C_{cyt} orientation of Ostβ-1–55, a tag containing a pair of *N*-glycosylation sites (denoted *N*N**) was fused to the N termini of 3×HA-tagged versions of Ostβ, Ostβ-1–55, Ostβ-1–55 R54A/R55A, and Ostβ-1–53 (Fig. 6*A*). The glycosylation tags on these constructs can only be modified if the protein is inserted in the membrane of the ER during translation with a N_{exo}/C_{cyt} orien-

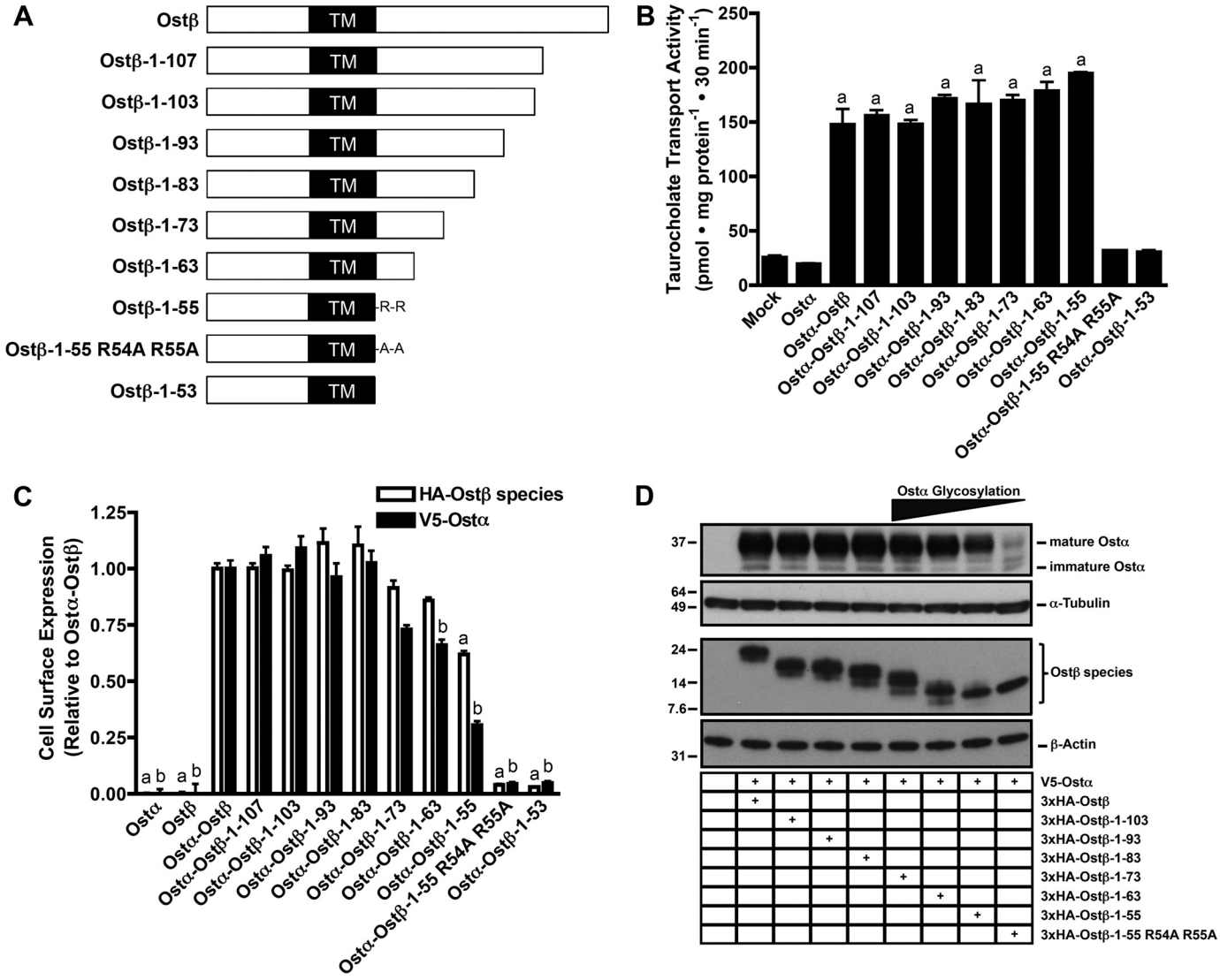

FIGURE 5. **Effects from C-terminal truncation of Ostβ.** *A*, Ostβ C-terminal truncations. *Letters* after the TM domain (*black bar*) denote residues remaining in the C terminus. *B*, [^{3}H]taurocholate transport activity produced by Ostα and the indicated Ostβ C-terminal truncations. *a*, $p < 0.05$ *versus* mock-transfected cells. *Error bars*, S.E. *C*, relative cell surface expression of V5-Ostα and the 3×HA-Ostβ truncations determined by ELISA. *a*, $p < 0.05$ *versus* 3×HA-Ostβ when co-expressed with V5-Ostα; *b*, $p < 0.05$ *versus* V5-Ostα when co-expressed with 3×HA-Ostβ. *D*, immunoblots of V5-Ostα and the 3×HA-Ostβ C-terminal truncations.

tation. Constructs were co-expressed with V5-Ostα, and the extent of glycosylation was determined by analyzing samples with and without enzymatic deglycosylation by PNGase F. As expected based on previous Ostβ topology studies (5), the *N*-glycosylation tag was highly modified on *N*N**-3×HA-Ostβ, which exhibited a sizeable molecular weight shift upon PNGase F treatment (Fig. 6*B*). *N*N**-3×HA-Ostβ-1–55 was also glycosylated, but neither *N*N**-3×HA-Ostβ-1–55 R54A/R55A nor *N*N**-3×HA-Ostβ-1–53 appeared to be (Fig. 6*B*). The intensity of the glycosylated V5-Ostα band was lower when V5-Ostα was co-expressed with *N*N**-3×HA-Ostβ-1–55 than with wild-type *N*N**-3×HA-Ostβ and negligible when it was co-expressed with the corresponding versions of Ostβ-1–55 R54A/R55A and Ostβ-1–53, although all of the Ostβ constructs expressed well. These findings indicate that Arg^{54} and Arg^{55} are important for Ostβ membrane orientation.

DISCUSSION

Ostα-Ostβ is a unique bile acid and steroid conjugate transporter composed of two distinct subunits that interact to generate the functional transporter. The current observations indicate that Ostβ not only modulates Ostα glycosylation, membrane trafficking, and turnover rate (5, 9) but also participates in the transport mechanism. The overall structure of the Ost transporter, in which a larger multi-TM domain subunit is accompanied by a single TM accessory protein, occurs frequently in membrane proteins. Examples include certain G protein-coupled receptors, like Frizzled-LRP5/6, CRLR-RAMP1, and MC2R-MRAP (34, 35); the nicotinic acetylcholine receptor, α7-nAchR-RIC-3 (36, 37); the K^+ channel, K_v1.4-K_vβ3 (38, 39); the Na^+/K^+-ATPase, ATP1A1-ATP1B1 (40, 41); and system L of the heterodimeric amino acid transporters, LAT1/2–4F2hc (42, 43). The single TM accessory proteins fulfill several functions, including (i) assisting with the folding of

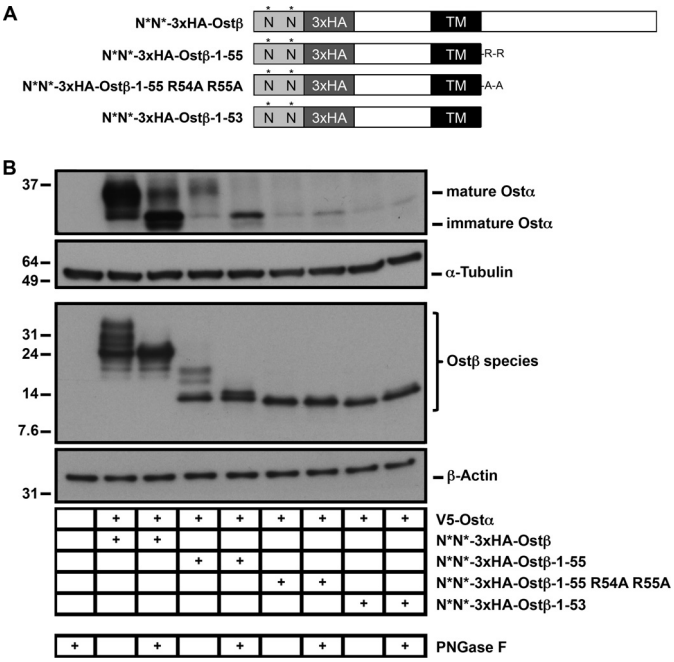

FIGURE 6. **Membrane orientation of Ostβ constructs.** *A*, Ostβ C-terminal truncations used in the N_{exo}/C_{cyt} topology assay. The relative positions of the *N*-glycosylation tag containing two sites for *N*-linked glycosylation (*N**) (*light gray bar*), the 3×HA epitope tag (*gray bar*), and the TM domain (*black bar*) are illustrated for each Ostβ mutant. *B*, analysis of glycosylation. Lysates from cells expressing the indicated constructs were treated with PNGase F or vehicle and analyzed via immunoblotting.

the larger subunit(s), (ii) escorting the larger subunit(s) to the plasma membrane, (iii) forming part of the active complex and assisting in its retention at the membrane, (iv) forming part of the ligand/substrate binding pocket, and (v) participating in desensitization and internalization.

The studies described here were designed to dissect the functions of different regions of Ostβ using a mutational strategy. The ability of Ostβ mutants to interact with Ostα was evaluated by BiFC, analysis of post-translational modification of Ostα, and determination of the stability of the individual subunits. The effect of mutations in Ostβ on trafficking of the Ostα-Ostβ complex to the plasma membrane was monitored via localization of fluorescently labeled Ostα and Ostβ using confocal microscopy and quantification of Ostα and Ostβ on the cell surface using ELISA. Finally, the impact of Ostβ mutations on the transport function of Ostα-Ostβ complexes was assessed by [^{3}H]taurocholate uptake. This multifaceted approach allowed specific roles to be assigned to distinct regions of the essential Ostβ subunit of the Ost heteromer.

Role of N Terminus and TM Domain of Ostβ—Mouse Ostβ has 34 amino acids in the extracellular N-terminal domain, including a highly conserved Asp-His-Ser sequence immediately following the initiating Met and a conserved region preceding the transmembrane helix. Ostβ-28–128, which lacks nearly all of the N terminus, was competent to deliver the complex to the plasma membrane and to generate transport activity, but only if cells were cultured at 30 °C.

Co-immunoprecipitation and BiFC experiments have established that Ostα and Ostβ form a tight complex when they are initially synthesized in the ER and remain associated in the functional transporter at the cell surface. Seward *et al.* (4) proposed that only a few conserved amino acids are required for interaction between Ostα and Ostβ. Skate Ostβ has just 25% amino acid identity with the human ortholog, yet these two proteins generate similar transport activity when co-expressed with human OSTα. Although the overall Ostβ amino acid identity is low among species (1), the Ostβ TM region from evolutionarily divergent species exhibits >40% amino acid identity, suggesting that the TM domain is a key element for heterodimerization and transport activity.

The present findings support this hypothesis by demonstrating that the TM domain of Ostβ is required for formation of a heteromer with Ostα. When the TM domain was deleted, yielding Ostβ-Δ34–53, no transport activity was detected upon co-expression with Ostα, and no interaction between the subunits was found by BiFC. Ostβ-Δ34–53-Topaz was distributed evenly throughout the cytoplasm. Ostβ-Δ34–53 could in theory have interacted with Ostα in BiFC experiments even though the two proteins were synthesized in different compartments of the cell because the YFP fragment was fused onto the cytoplasmic side of Ostα. The failure of Ostα and Ostβ-Δ34–53 to interact may explain why both proteins were largely undetectable on immunoblots; native Ostα and Ostβ are both unstable when expressed alone. Stronger evidence supporting the importance of the TM domain is provided by Ostβ-W34A/N35A, a TM domain mutant that did not generate any transport activity although it did localize at the cell surface and interact with Ostα in BiFC experiments. The functional deficit of Ostβ-W34A/N35A and Ostα cannot be explained by the 25–50% decrease in the amount of the subunits at the plasma membrane, because cell surface levels of Ostα-Ostβ-1–55 were much lower, and yet this complex exhibited normal transport activity. Taken together, the data provide compelling evidence that the TM domain of Ostβ, in particular the Trp-Asn sequence at the extracellular-membrane interface, is directly involved in the transport mechanism. When present in TM helices, Trp and Asn are often found near the membrane-water interface where they are more energetically favorable and confer stability to a TM helix (44, 45). Asn can form hydrogen bonds with the peptide backbone (*i.e. N*-capping) to stabilize an α-helix (46) and drive TM-TM interactions via hydrogen bonding (47–51), which may occur between Ostα and Ostβ.

Because the Ostα-Ostβ-29–53 complex gave a BiFC signal, the TM domain of Ostβ was sufficient for interaction with Ostα, but it was not sufficient for trafficking to the cell surface. In fact, no single site within Ostβ was found to be solely responsible for membrane trafficking of the heteromeric complex. Therefore, it is likely that other sites of interaction between the subunits exist and facilitate membrane trafficking of the transporter. In support of this, Sun *et al.* (10) demonstrated that the 50 N-terminal residues of human OSTα are required for interaction with human OSTβ and in turn trafficking of the transporter complex to the plasma membrane. The stoichiometry of the Ost transporter is unknown. Ostα forms homodimers (5), and it is possible that interaction between two Ostα subunits is dependent on Ostβ and essential for trafficking.

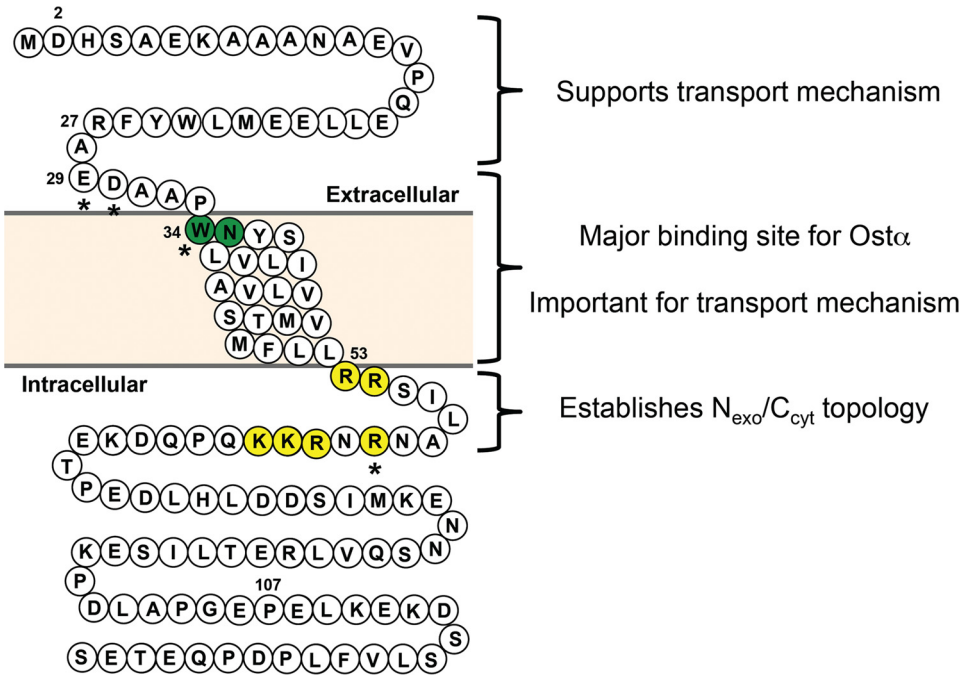

FIGURE 7. **Proposed function(s) of Ostβ regions.** Proposed functions of different regions of Ostβ are shown schematically. The TM region appears to be sufficient and necessary for interaction with Ostα. The Trp-Asn residues shown in *green* are essential for transport activity, and the positively charged residues shown in *yellow* are important for establishing the N_{exo}/C_{cyt} topology of Ostβ. *Asterisks* denote fully conserved residues.

Role of Positively Charged Residues in C Terminus of Ostβ—Ostβ is a type Ia integral membrane protein with a N_{exo}/C_{cyt} topology (5). A stretch of 7–25 amino acids, which are uncharged and largely hydrophobic, constitutes a signal sequence (often a TM domain) that targets an integral membrane protein to the ER for co-translational insertion (52). Several factors influence the orientation of a signal sequence in the ER membrane and in turn establish the topology of the integral membrane protein. Most important is the positive inside rule, which states that the positively charged residues flanking the signal sequence determine its membrane orientation such that the more positive flank faces the cytoplasm. When the 15 N-terminal and C-terminal residues flanking a signal sequence are analyzed, the cytoplasmic end usually contains ~2–3-fold higher frequency of Arg+Lys residues than the end facing the ER lumen (30–33). Ostβ appears to abide by this rule, because the 15 residues C-terminal to the TM domain contain six positively charged amino acids whereas the extracellular 15 N-terminal residues have only one (5).

This positive charge distribution explains the cell surface localization of Ostβ mutants with C-terminal truncations. As the C terminus was shortened, the proteins had less positive charge on the C-terminal side of the TM; there were 6, 4, 2 and 0 Lys+Arg residues in wild type, 1–63, 1–55, and 1–53 or 1–55 R54A/R55A Ostβ, respectively. Based on the absence of modification on their *N*-glycosylation tags, Ostβ-1–53 and Ostβ-1–55 R54A/R55A were inserted in the ER membrane upside down (N_{cyt}/C_{exo}) and did not support trafficking or function of the transporter unit. This probably occurred because the incorrectly oriented Ostβs did not interact with Ostα, which was therefore degraded. When Ostβ-1–53 was fused to YC or Topaz, the truncated Ostβ regained the ability to interact with Ostα, traffic to the plasma membrane and generate transport activity. The gain of functional activity is most likely explained by the increase in positive charge on the C-terminal side introduced by the tags (2 Arg+Lys) and the tendency of folded domains such as YC/Topaz to localize to the cytoplasmic side.

The novel findings presented here are summarized in Fig. 7, which illustrates the regions of Ostβ and their proposed function(s). Mutations in several highly conserved amino acids did not, by themselves, disrupt Ostβ activity. The N terminus of Ostβ may be necessary for correct folding and/or assembly of the transporter, but if this requirement is bypassed by low temperature incubation, a transporter missing all but 5 amino acids N-terminal to the TM domain yields robust transport activity. Residues on the C-terminal side of the TM domain (*yellow*) are necessary for correct membrane orientation of Ostβ, which is essential for Ostα-Ostβ interaction. If this requirement is bypassed, however, then a transporter lacking the entire C-terminal domain can generate functional activity. Thus, all of the results obtained here point to the highly conserved TM domain region of Ostβ as the major site of interaction with Ostα. The TM helix also appears to be part of the functional component of the holotransporter, and the evolutionarily conserved Trp-Asn (W34/N35) sequence at the extracellular N terminus of the helix is absolutely required for transport activity. It is likely that future studies on the biochemistry of the transporter complex will identify additional contributions of the N- and C-terminal domains of Ostβ and more specific roles of the TM helix. Because of the potential benefits of drugs targeting the Ost transporter *in vivo*, detailed understanding of the role of the subunits should be of great value.

Acknowledgments—We thank Dr. Tom K. Kerppola, University of Michigan Medical School, Ann Arbor, MI, for providing BiFC plasmids, and Dr. Linda Callahan, Director of the Confocal and Conventional Microscropy Core at the University of Rochester, Rochester, NY, for assistance with confocal microscopy imaging.

REFERENCES

1. Ballatori, N., Li, N., Fang, F., Boyer, J. L., Christian, W. V., and Hammond, C. L. (2009) Ostα-Ostβ: a key membrane transporter of bile acids and conjugated steroids. *Front. Biosci*. **14,** 2829–2844
2. Soroka, C. J., Ballatori, N., and Boyer, J. L. (2010) Organic solute transporter, Ostα-Ostβ: its role in bile acid transport and cholestasis. *Semin. Liver Dis.* **30,** 178–185
3. Ballatori, N. (2011) Pleiotropic functions of the organic solute transporter Ostα-Ostβ. *Dig. Dis.* **29,** 13–17
4. Seward, D. J., Koh, A. S., Boyer, J. L., and Ballatori, N. (2003) Functional complementation between a novel mammalian polygenic transport complex and an evolutionarily ancient organic solute transporter, Ostα-Ostβ. *J. Biol. Chem.* **278,** 27473–27482
5. Li, N., Cui, Z., Fang, F., Lee, J. Y., and Ballatori, N. (2007) Heterodimerization, trafficking and membrane topology of the two proteins, Ostα and Ostβ, that constitute the organic solute and steroid transporter. *Biochem. J.* **407,** 363–372
6. Ballatori, N., Fang, F., Christian, W. V., Li, N., and Hammond, C. L. (2008) Ostα-Ostβ is required for bile acid and conjugated steroid disposition in the intestine, kidney, and liver. *Am. J. Physiol. Gastrointest. Liver Physiol.* **295,** G179–186
7. Rao, A., Haywood, J., Craddock, A. L., Belinsky, M. G., Kruh, G. D., and Dawson, P. A. (2008) The organic solute transporter α-β, Ostα-Ostβ, is essential for intestinal bile acid transport and homeostasis. *Proc. Natl. Acad. Sci. U.S.A.* **105,** 3891–3896
8. Trauner, M., and Boyer, J. L. (2003) Bile salt transporters: molecular characterization, function, and regulation. *Physiol. Rev.* **83,** 633–671
9. Dawson, P. A., Hubbert, M., Haywood, J., Craddock, A. L., Zerangue, N., Christian, W. V., and Ballatori, N. (2005) The heteromeric organic solute transporter α-β, Ostα-Ostβ, is an ileal basolateral bile acid transporter. *J. Biol. Chem.* **280,** 6960–6968
10. Sun, A. Q., Balasubramaniyan, N., Xu, K., Liu, C. J., Ponamgi, V. M., Liu, H., and Suchy, F. J. (2007) Protein-protein interactions and membrane localization of the human organic solute transporter. *Am. J. Physiol. Gastrointest. Liver Physiol.* **292,** G1586–1593
11. Wang, W., Seward, D. J., Li, L., Boyer, J. L., and Ballatori, N. (2001) Expression cloning of two genes that together mediate organic solute and steroid transport in the liver of a marine vertebrate. *Proc. Natl. Acad. Sci. U.S.A.* **98,** 9431–9436
12. Ballatori, N., Christian, W. V., Lee, J. Y., Dawson, P. A., Soroka, C. J., Boyer, J. L., Madejczyk, M. S., and Li, N. (2005) Ostα-Ostβ: a major basolateral bile acid and steroid transporter in human intestinal, renal, and biliary epithelia. *Hepatology* **42,** 1270–1279
13. Hu, C. D., Chinenov, Y., and Kerppola, T. K. (2002) Visualization of interactions among bZIP and Rel family proteins in living cells using bimolecular fluorescence complementation. *Mol. Cell* **9,** 789–798
14. Kerppola, T. K. (2006) Design and implementation of bimolecular fluorescence complementation (BiFC) assays for the visualization of protein interactions in living cells. *Nat. Protoc.* **1,** 1278–1286
15. Kerppola, T. K. (2006) Complementary methods for studies of protein interactions in living cells. *Nat. Methods* **3,** 969–971
16. Tsien, R. Y. (1998) The green fluorescent protein. *Annu. Rev. Biochem.* **67,** 509–544
17. Gehret, A. U., Jones, B. W., Tran, P. N., Cook, L. B., Greuber, E. K., and Hinkle, P. M. (2010) Role of helix 8 of the thyrotropin-releasing hormone receptor in phosphorylation by G protein-coupled receptor kinase. *Mol. Pharmacol.* **77,** 288–297
18. Harley, C. A., Holt, J. A., Turner, R., and Tipper, D. J. (1998) Transmembrane protein insertion orientation in yeast depends on the charge difference across transmembrane segments, their total hydrophobicity, and its distribution. *J. Biol. Chem.* **273,** 24963–24971
19. Kaufmann, H., Mazur, X., Fussenegger, M., and Bailey, J. E. (1999) Influence of low temperature on productivity, proteome and protein phosphorylation of CHO cells. *Biotechnol. Bioeng.* **63,** 573–582
20. Fox, S. R., Tan, H. K., Tan, M. C., Wong, S. C., Yap, M. G., and Wang, D. I. (2005) A detailed understanding of the enhanced hypothermic productivity of interferon-γ by Chinese hamster ovary cells. *Biotechnol. Appl. Biochem.* **41,** 255–264
21. Galbraith, D. J., Tait, A. S., Racher, A. J., Birch, J. R., and James, D. C. (2006) Control of culture environment for improved polyethylenimine-mediated transient production of recombinant monoclonal antibodies by CHO cells. *Biotechnol. Prog.* **22,** 753–762
22. Geisse, S., and Fux, C. (2009) Recombinant protein production by transient gene transfer into mammalian cells. *Methods Enzymol.* **463,** 223–238
23. Ljunggren, H. G., Stam, N. J., Ohlén, C., Neefjes, J. J., Höglund, P., Heemels, M. T., Bastin, J., Schumacher, T. N., Townsend, A., and Kärre, K. (1990) Empty MHC class I molecules come out in the cold. *Nature* **346,** 476–480
24. Denning, G. M., Anderson, M. P., Amara, J. F., Marshall, J., Smith, A. E., and Welsh, M. J. (1992) Processing of mutant cystic fibrosis transmembrane conductance regulator is temperature-sensitive. *Nature* **358,** 761–764
25. Powell, K., and Zeitlin, P. L. (2002) Therapeutic approaches to repair defects in ΔF508 CFTR folding and cellular targeting. *Adv. Drug Deliv. Rev.* **54,** 1395–1408
26. Bokman, S. H., and Ward, W. W. (1981) Renaturation of Aequorea green fluorescent protein. *Biochem. Biophys. Res. Commun.* **101,** 1372–1380
27. Corish, P., and Tyler-Smith, C. (1999) Attenuation of green fluorescent protein half-life in mammalian cells. *Protein Eng.* **12,** 1035–1040
28. Chiang, C. F., Okou, D. T., Griffin, T. B., Verret, C. R., and Williams, M. N. (2001) Green fluorescent protein rendered susceptible to proteolysis: positions for protease-sensitive insertions. *Arch. Biochem. Biophys.* **394,** 229–235
29. March, J. C., Rao, G., and Bentley, W. E. (2003) Biotechnological applications of green fluorescent protein. *Appl. Microbiol. Biotechnol.* **62,** 303–315
30. Heijne, G. (1986) The distribution of positively charged residues in bacterial inner membrane proteins correlates with the trans-membrane topology. *EMBO J.* **5,** 3021–3027
31. von Heijne, G., and Gavel, Y. (1988) Topogenic signals in integral membrane proteins. *Eur. J. Biochem.* **174,** 671–678
32. Sipos, L., and von Heijne, G. (1993) Predicting the topology of eukaryotic membrane proteins. *Eur. J. Biochem.* **213,** 1333–1340
33. Goder, V., and Spiess, M. (2001) Topogenesis of membrane proteins: determinants and dynamics. *FEBS Lett.* **504,** 87–93
34. He, X., Semenov, M., Tamai, K., and Zeng, X. (2004) LDL receptor-related proteins 5 and 6 in Wnt/β-catenin signaling: arrows point the way. *Development* **131,** 1663–1677
35. Cooray, S. N., Chan, L., Webb, T. R., Metherell, L., and Clark, A. J. (2009) Accessory proteins are vital for the functional expression of certain G protein-coupled receptors. *Mol. Cell. Endocrinol.* **300,** 17–24
36. Wang, Y., Yao, Y., Tang, X. Q., and Wang, Z. Z. (2009) Mouse RIC-3, an endoplasmic reticulum chaperone, promotes assembly of the α7 acetylcholine receptor through a cytoplasmic coiled-coil domain. *J. Neurosci.* **29,** 12625–12635
37. Yang, K. C., Jin, G. Z., and Wu, J. (2009) Mysterious α6-containing nAChRs: function, pharmacology, and pathophysiology. *Acta Pharmacol. Sin.* **30,** 740–751
38. Castellino, R. C., Morales, M. J., Strauss, H. C., and Rasmusson, R. L. (1995) Time- and voltage-dependent modulation of a $K_v1.4$ channel by a β-subunit ($K_v\beta3$) cloned from ferret ventricle. *Am. J. Physiol.* **269,** H385–391
39. Dolly, J. O., and Parcej, D. N. (1996) Molecular properties of voltage-gated K^+ channels. *J. Bioenerg. Biomembr.* **28,** 231–253
40. Gorokhova, S., Bibert, S., Geering, K., and Heintz, N. (2007) A novel family of transmembrane proteins interacting with β-subunits of the Na,K-ATPase. *Hum. Mol. Genet.* **16,** 2394–2410
41. Morth, J. P., Pedersen, B. P., Buch-Pedersen, M. J., Andersen, J. P., Vilsen, B., Palmgren, M. G., and Nissen, P. (2011) A structural overview of the

plasma membrane Na^+,K^+-ATPase and H^+-ATPase ion pumps. *Nat. Rev. Mol. Cell. Biol.* **12,** 60–70
42. Verrey, F., Meier, C., Rossier, G., and Kühn, L. C. (2000) Glycoprotein-associated amino acid exchangers: broadening the range of transport specificity. *Pflugers Arch.* **440,** 503–512
43. Meier, C., Ristic, Z., Klauser, S., and Verrey, F. (2002) Activation of system L heterodimeric amino acid exchangers by intracellular substrates. *EMBO J.* **21,** 580–589
44. Ulmschneider, M. B., and Sansom, M. S. (2001) Amino acid distributions in integral membrane protein structures. *Biochim. Biophys. Acta* **1512,** 1–14
45. Mackinnon, R. (2005) Structural biology: membrane protein insertion and stability. *Science* **307,** 1425–1426
46. Richardson, J. S., and Richardson, D. C. (1988) Amino acid preferences for specific locations at the ends of α-helices. *Science* **240,** 1648–1652
47. Dawson, J. P., Melnyk, R. A., Deber, C. M., and Engelman, D. M. (2003) Sequence context strongly modulates association of polar residues in transmembrane helices. *J. Mol. Biol.* **331,** 255–262
48. Choma, C., Gratkowski, H., Lear, J. D., and DeGrado, W. F. (2000) Asparagine-mediated self-association of a model transmembrane helix. *Nat. Struct. Biol.* **7,** 161–166
49. Zhou, F. X., Cocco, M. J., Russ, W. P., Brunger, A. T., and Engelman, D. M. (2000) Interhelical hydrogen bonding drives strong interactions in membrane proteins. *Nat. Struct. Biol.* **7,** 154–160
50. Gratkowski, H., Lear, J. D., and DeGrado, W. F. (2001) Polar side chains drive the association of model transmembrane peptides. *Proc. Natl. Acad. Sci. U.S.A.* **98,** 880–885
51. Zhou, F. X., Merianos, H. J., Brunger, A. T., and Engelman, D. M. (2001) Polar residues drive association of polyleucine transmembrane helices. *Proc. Natl. Acad. Sci. U.S.A.* **98,** 2250–2255
52. Higy, M., Junne, T., and Spiess, M. (2004) Topogenesis of membrane proteins at the endoplasmic reticulum. *Biochemistry* **43,** 12716–12722